

A BASIC STUDY ON SOIL MOISTURE ALGORITHM USING GROUND-BASED OBSERVATIONS UNDER DRY CONDITION

Hui LU¹, Toshio KOIKE², Nozomu HIROSE³, Masato MORITA⁴, Hideyuki FUJII³,
David Ndegwa KURIA⁵, Tobias GRAF³ and Hiroyuki TSUTSUI⁶

¹Student Member of JSCE, Doctoral Student, Dept. of Civil Eng., Univ. of Tokyo (Bunkyo-ku, Tokyo 113-8656, Japan)

²Member of JSCE, Dr. Eng., Professor, Dept. of Civil Eng., Univ. of Tokyo (Bunkyo-ku, Tokyo 113-8656, Japan)

³Member of JSCE, Dr. Eng., Dept. of Civil Eng., Univ. of Tokyo (Bunkyo-ku, Tokyo 113-8656, Japan)

⁴Research, Dept. of Civil Eng., Univ. of Tokyo (Bunkyo-ku, Tokyo 113-8656, Japan)

⁵Doctoral Student, Dept. of Civil Eng., Univ. of Tokyo (Bunkyo-ku, Tokyo 113-8656, Japan)

⁶Member of JSCE, M. Eng., Dept. of Civil Eng., Univ. of Tokyo (Bunkyo-ku, Tokyo 113-8656, Japan)

Ground-based microwave radiometric field observations were conducted by using the Ground Based Passive Microwave Radiometer (GBMR) at frequencies of 6.9, 10.65 and 18.7 GHz to gain a better understanding of the physical mechanism of the radiative transfer process taken place in dry soil media. A metal plate was used as a bottom boundary and dry soil was put on it by increasing its depth one centimeter by one centimeter. The observed brightness temperature increased as the dry soil depth increased, while the increment of brightness temperature per one centimeter increase of soil depth was getting smaller. This behavior demonstrated the existence of volume scattering effects in the dry soil. Three models: surface emission model, Mie-scattering model and dense media radiative transfer model, were applied to the experiment results. The dense media radiative transfer model shows the best agreement with the observed data.

Key Words: *Ground Based Passive Microwave Radiometer, Soil Moisture, Microwave Remote Sensing, Dense Media Radiative Transfer Theory*

1. INTRODUCTION

Soil moisture plays a critical role in the global energy and water balance, e.g. it decides the ratio of runoff and infiltration of catchments and supplies water for the evaporation. However, due to its large variability, it is very difficult to observe the spatial and temporal distribution of soil moisture in a large scale by in situ measurements. As a result, in recent 30 years, much effort has been directed towards observing soil moisture by satellite remote sensing techniques.

Due to the characters of long wavelength in microwave region and independent of illumination source, satellite passive microwave remote sensing has the advantage to monitor the soil moisture in a large scale. Heretofore, many algorithms have been developed and products of them are not used widely^{1, 2)}, because the accuracy of retrieved soil

moisture is far from satisfactory. One of the key reasons of the low accuracy is the volume scattering effects of soil particles, which becomes bigger in dry cases³⁾.

The objective of our study is to develop a radiative transfer model to represent the physical truth of radiative transfer process which taken place in dry soil media. In order to evaluate and improve radiative transfer models for soil, field experiments were designed to create a detailed data set of radiometric observations of dry soil, and have been carried out from February to May 2005 in the Field Production Science Center in Graduate School of Agricultural and Life Sciences in the University of Tokyo (UTFPSC), Tokyo, Japan.

The paper is consisting of five parts. After the introduction, the experiment set-up and the observations are introduced. The third part provides an analysis of the field experiment results.

Afterwards three radiative transfer models are briefly introduced and simulating results are presented and compared with the field observation. The paper concludes with some final remarks.

2. OBSERVATION

The main goal of the field experiments was to create a data set, which can be used to evaluate and improve radiative transfer models, by observing the brightness temperature of dry soil and its physical temperature and water content simultaneously.

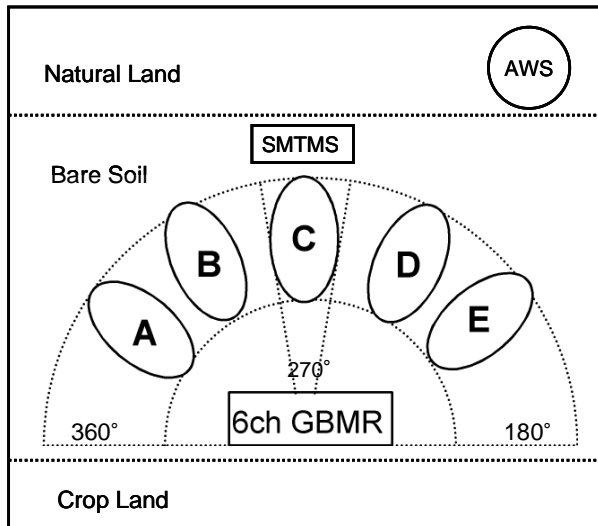


Fig. 1 Overview of Instrument Set-Up

(1) Site Overview

Fig. 1 provides an overview of the instrument set-up. The ground based microwave radiometer system has been installed at the edge of experiment field. The location for soil moisture and temperature measurement system (SMTMS) and the automatic weather station (AWS) have been selected, so that they are close to the radiometer footprints.

The observed target at azimuth angle of 310° is footprint A, 290° is footprint B, 270° is footprint C, 250° is footprint D and 230° is footprint E, respectively. Three different scan areas have been selected to observe the brightness temperature of soil in different situations:

Footprint C – Undisturbed bare soil: The bare soil in this area was undisturbed during whole observation period and therefore it represented the natural status of bare soil.

Footprint B – Dry soil on the metal plate: In this area the dry soil was added onto the metal plate by increasing its depth one centimeter by one centimeter to observe impacts of bare soil emission and volume scattering on the brightness temperature.

Footprint A, D, E – Reference bare soil: In this area the surface is leveled before every measurement.

(2) Ground Based Microwave Radiometer

The ground based brightness temperature observations have been implemented by means of the 6 channel Ground Based Microwave Radiometer (GBMR-6). The GBMR-6 is a dual polarization, multi-frequency passive microwave radiometer, which observes the brightness temperature at 6.925, 10.65 and 18.7 GHz. The radiometer was developed to provide frequencies similar to those of the Advanced Microwave Scanning Radiometers for EOS (AMSR-E) on Aqua and AMSR on ADEOS-II.

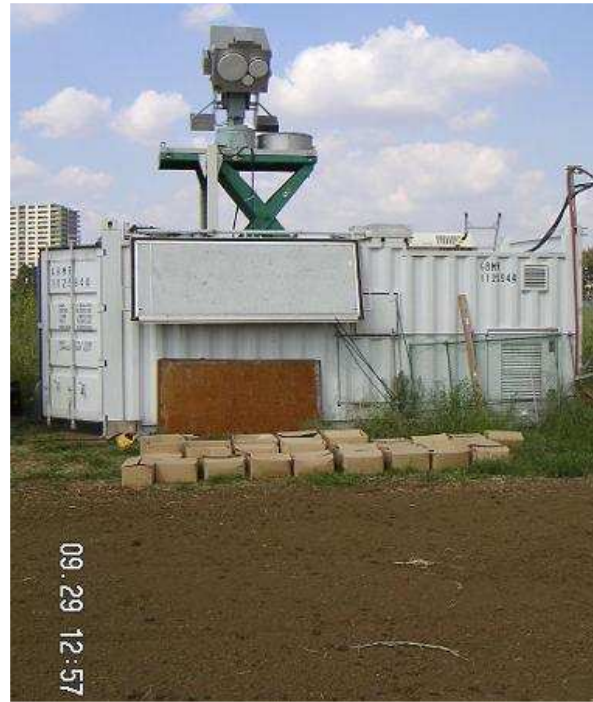


Fig. 2 GBMR-6 at the experiment filed of UTFPSC, Tokyo, Japan

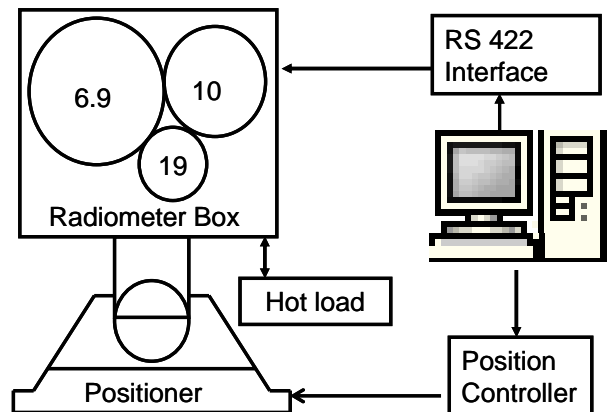


Fig. 3 Diagram of the GBMR-6 Components and Connections

Fig. 2 is a picture of the radiometer at the experiment site of UTFPSC. The radiometers are equipped in the Radiometer Box which provides a temperature stabilized environment. The box is mounted on a positioner which allows movement of 0° to 360° in azimuth and -90° to 90° in elevation⁴⁾.

Fig. 3 provides a block diagram of components and connections of the GBMR-6 system.

The calibration of the GBMR-6 is based on external reference targets: a hot load and a cold load. The hot load is the microwave absorber at ambient temperature which is equipped inside of a vessel. Liquid nitrogen, which is stored in a vessel lined with the microwave absorber, is used as the cold load. The measurement range of GBMR-6 is from 0K to 350K with an absolute accuracy of 0.5K.

The GBMR-6 is operated by a personal computer. The software monitors the status of radiometers, controls the positioner, and collects data. Observation can be implemented as one footprint observation or multi-footprint observation. For multi-footprint observation, the system can be set to make observations according to the specified scan files.

(3) Soil temperature and moisture measurement

The Soil Moisture and Temperature Measurement System (SMTMS) was installed for simultaneous measurement of soil moisture and temperature profiles. The SMTMS used in this study have ten temperature probes and six soil moisture probes. Those probes were attached to the interested footprints and metal plates.

Soil samples were taken after every measurement to obtain the soil density and water content. The infrared thermometer was used for the measurement of surface temperature of interested footprints.

The automated weather station (AWS) was installed to continuously monitor the meteorological conditions at the site.

(4) Experiment procedure

The field observation was processed as following:

- (1) Drying soil in the oven at 80 ° C to make the soil very dry.
- (2) Covering the footprint B with a metal plate and leveling the reference footprints A and D
- (3) Measuring the brightness temperature of all five footprints by using GBMR at a fixed incident angle of 55°, which is similar to that of the AMSR and AMSR-E sensors.
- (4) Collecting soil moisture and temperature data and soil samples.
- (5) Measuring the sky radiation at the incident angle 55°
- (6) Increasing the soil depth with one centimeter on the metal plate and making a smooth surface
- (7) Repeat step 3-6 till using up the dry soil or accessing the brightness temperature saturation.

After each observation, the surface roughness of footprint B was measured by a metallic-needle profilometer, then the height standard deviation and

correlation length were calculated to check whether the surface was specular or not.

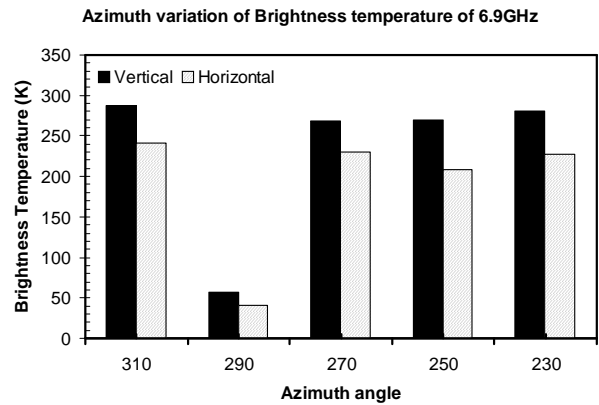


Fig. 4 Azimuth Variation of Brightness Temperature of Initial Situation at 6.9 GHz

3. OBSERVED RESULTS OF FIELD EXPERIMENTS

Fig. 4 shows the observed brightness temperature of the five targets at the two polarizations at 6.9GHz. Due to the high reflectivity of the metal plate, the observed brightness temperature of the footprint B is much lower than that of other footprints. By assuming a specular surface of the metal plate, the effective reflectivity of the metal plate is calculated as:

$$\Gamma_e = \frac{T_{phy} - TB}{T_{phy} - T_{sky}} \quad (1)$$

where Γ_e is the effective reflectivity of metal plates, T_{phy} the physical temperature of the metal plate in Kelvin, TB observed brightness temperature of the metal plate by GBMR-6, and T_{sky} brightness temperature of sky radiation at the incident angle 55°.

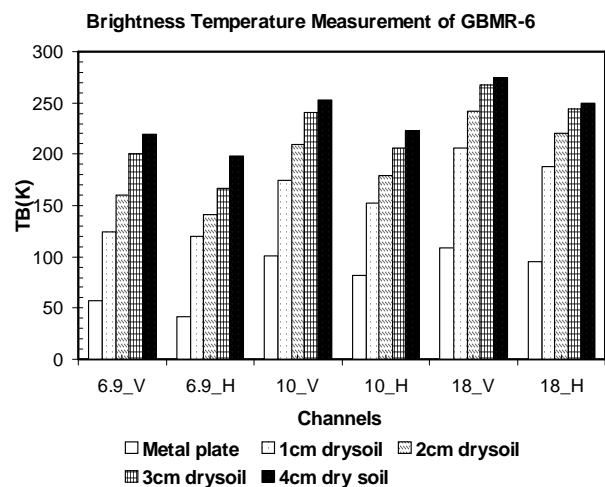


Fig. 5 Brightness Temperature Measurement of GBMR-6 at footprint B

Fig. 5 Shows the changes of the brightness temperature at 6.9, 10.65 and 18.7 GHz (both vertical and horizontal polarization) due to the increase of soil depth. From **Fig. 5**, it is obviously that the brightness temperature of the footprint B increases as the soil depth increases. This brightness temperature increment is mainly due to the emission effects of dry soil layer. And when we added dry soil continually on the footprint B, the increment of brightness temperature due to the newly addressed one centimeter dry soil was getting smaller. This phenomenon is due to the volumetric scattering extinction effect of the dry soil particles. The scattering effect increases as the number of scatterers and their size increases. Furthermore the smaller increment of the brightness temperature is clearer at the higher frequency in **Fig. 5**.⁵⁾

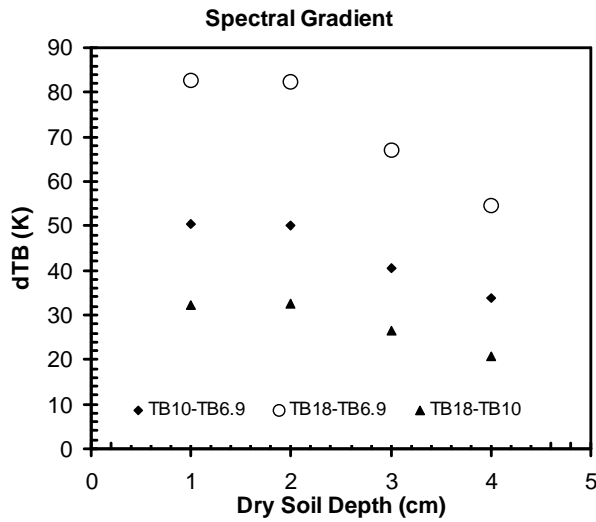


Fig. 6 Change of Spectral Gradient

The **Fig. 6** displays the brightness temperature difference among those three frequencies (vertical polarization), the so-called spectral gradient. The diamonds represent the brightness temperature difference between 10 GHz and 6.9 GHz; circles represent that between 18 GHz and 6.9 GHz, while triangles are showing that between 18GHz and 10 GHz. With the exception of the case of one centimeter depth, the results in **Fig. 6** show the spectral gradient decreases as the soil depth increases. It can be explained that because the higher frequency channels are more sensitive to the volume scattering effect of the dry soil than the lower frequency ones.

4. RADIATIVE TRANSFER MODEL

In order to improve the understanding of the radiative transfer process in dry soil media, three different radiative transfer models: surface emission model, Mie-scattering model and dense media

radiative transfer model, are applied to the observed data.

(1) Surface Emission Model

In this model, the soil is treated as an isothermal semi-infinite medium with a specular surface. It is widely used in many algorithms and the microwave brightness temperature is calculated by the model as follows:

$$TB = eT_{phy} + (1-e)T_{sky} \quad (2)$$

where e is the emissivity of the medium, and the meaning of other symbols is the same as in equation (1).

Emissivity is related to reflectivity Γ by $e=1-\Gamma$, while the reflectivity is calculated from Fresnel equations by assuming a specular surface⁶⁾. The dielectric constant of soil is calculated by using the Dobson model⁷⁾, and the dielectric constant of water is calculated following P.S. Ray equations⁸⁾.

(2) Mie-scattering Model

Mie-scattering model treats soil medium as a slab containing many spherical soil particles overlaying a boundary with a reflectivity of Γ_e calculated from equation (1). The radiative transfer process in the soil slab is simulated by the discrete ordinate method (4 streams)⁹⁾ and the Henyey-Greenstein phase function¹⁰⁾ in this study.

In Mie-scattering model, the volume scattering coefficient k_s and absorption coefficient k_a can be calculated as

$$k_s = \sum_{i=1}^N N_i \cdot \sigma_{s,i} \quad (3)$$

$$k_a = \sum_{i=1}^N N_i \cdot \sigma_{a,i} \quad (4)$$

where N_i represents the number density of the particle with size i and $\sigma_{s,i}$ and $\sigma_{a,i}$ the scattering and absorption cross section for a particle with size i . The scattering and absorption cross sections of soil particles are calculated using the Mie theory¹¹⁾.

(3) Dense Media Radiative Transfer Model

The dense medium radiative transfer model is very similar to the Mie-scattering model. The difference of the two models is that the Mie-scattering model does not consider the correlated scattering effects while the dense media radiative transfer model considers it.

The correlated scattering (multiple scattering) effect of densely packed particles is modeled by introducing the so-called dense media radiative transfer theory (DMRT) under the Quasi Crystalline Approximation with Coherent Potential (QCA-CP)^{12, 13)}. Dense Medium radiative transfer theory was derived from Dyson's equation under the quasi-crystalline approximation with coherent potential (QCA-CP) and the Bethe-Salpeter equation under

the ladder approximation of correlated scatterers. The numerical solutions of the dense radiative transfer equation are similar to those of the conventional radiative transfer method, provided that the extinction coefficient k_e and the single scattering albedo ω are introduced.

The extinction rate k_e is defined as:

$$k_e = 2\text{Im}(K) \quad (5)$$

while the effective propagation constant K satisfies the following equation:

$$K^2 \approx K'^2 + 2iK'K'' \\ = K_0^2 \left\{ 1 + i \frac{2}{9} \frac{K_0 a^3 (k_s^2 - k^2)}{1 + \frac{k_s^2 - k^2}{3K_0^2} (1-f)} \frac{(1-f)^4}{(1+2f)^2} \right\} \quad (6)$$

and

$$K_0^2 = k^2 + \frac{f(k_s^2 - k^2)}{1 + \frac{k_s^2 - k^2}{3K_0^2} (1-f)} \quad (7)$$

where k is the wave number in background, k_s the wave number in particles, and f the fractional volume occupied by particles.

The albedo ω is calculated as:

$$\omega = \frac{2}{9} \frac{a^3 f}{k_e} \left| \frac{k_s^2 - k^2}{1 + \frac{k_s^2 - k^2}{3K_0^2} (1-f)} \right|^2 \frac{(1-f)^4}{(1+2f)^2} \quad (8)$$

(4) Modeling Results

Fig. 7 shows the simulation results of three aforementioned models for all six channels' observation. The x-axis is the frequency and polarization. The circles are showing observed brightness temperatures. The squares represent the simulation results of the surface emission model, while triangles and stars represent those of the Mie-scattering model and the dense media radiative transfer model, respectively. The simulation results are obtained using simultaneously observed soil properties (temperature, water content, density and texture) as input parameters, with the only exception of the soil particle size, which is an important parameter used in Mie-scattering model and dense media model.

A soil particle size d for each frequency is decided in the case of 1cm depth through a best fitting way, which can be expressed as:

$$J = \sum (|Tb_{v,sim} - Tb_{v,obs}| + |Tb_{h,sim} - Tb_{h,obs}|) = f(d) \quad (9)$$

where J is the cost, $Tb_{v,sim}$ and $Tb_{h,sim}$ are brightness temperature calculated from the models, and $Tb_{v,obs}$ and $Tb_{h,obs}$ are the actual brightness temperature observed by GBMR-6. Through the minimizing the cost J , the best fitting value of soil particle size can be obtained. Table 1 shows the best fitting particle sizes for Mie-scattering model and dense media model using observation of one centimeter dry soil depth.

Table. 1 Best fitting values of particle size d (mm)

Freq.(GHz)	6.925	10.65	18.7
Mie-scattering	18	12	6
Dense Media	14	7	2.5

The values of best fitting particle size change at different frequencies, fitting the longer wavelength with the larger value.

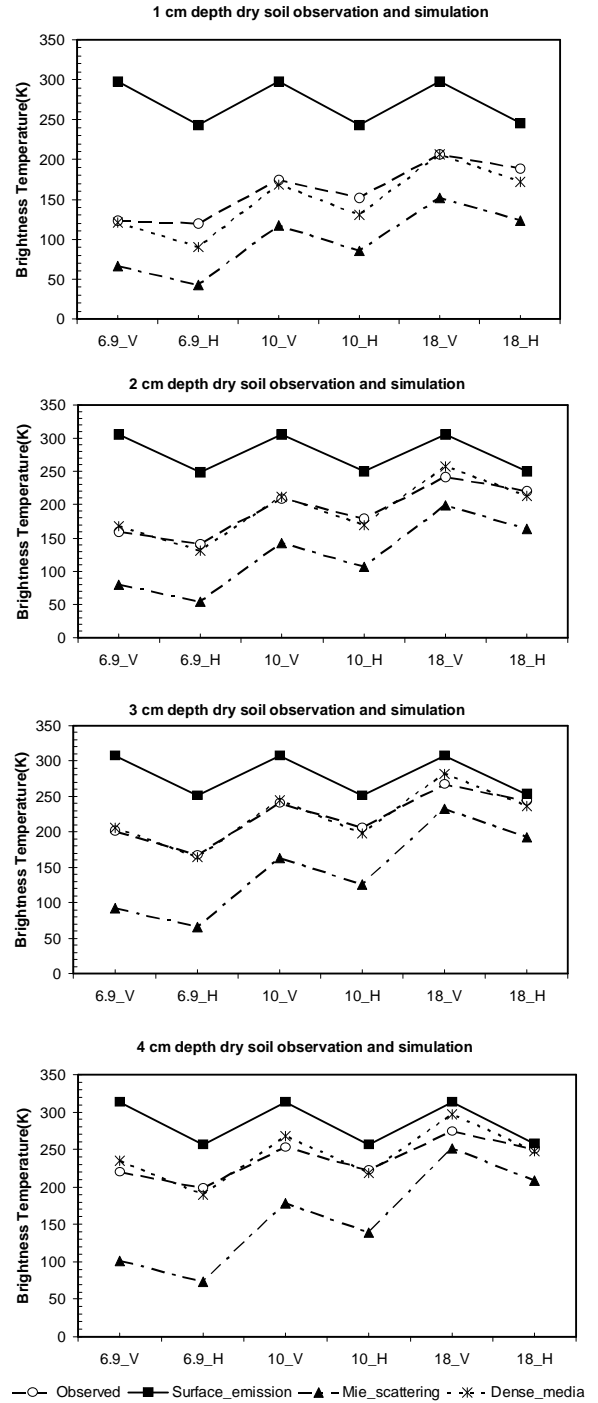


Fig. 7 Modeling results simulating by surface emission model, Mie-scattering model and dense media model

Fig. 7 shows that the dense media model is able to reproduce experimental data well for all the soil depth cases, while the Mie-scattering model underestimates the brightness temperature and the surface emission model overestimates it.

The difference between the simulated brightness temperature of surface emission model and the observed one is getting smaller at higher frequencies and larger soil depth. It is because that the penetration depth at higher frequency is smaller. When soil depth increases, it is easier for high frequency to get closer to the assumption of surface emission model: semi-infinite media without considering the existence of metal plate.

For Mie-scattering model, the difference between the simulated results and observed result is large for all frequencies. It is partly due to the relationship between particle size and particle number, which make Mie-scattering model fail to represent the absorption coefficient of soil media at this frequencies range and therefore we can not increase brightness temperature as particle size d increases.

The accuracy of the dense media model decreases as frequency and soil depth increase. One of the reasons of this estimation error is caused by inaccurate arrangement of the soil depth on the metal plate in this experiment. The soil depth inhomogeneity in the footprint B became larger, as the soil depth increased. Such uncertainty results in the larger errors at higher frequency, which is more sensitive to the volume scattering effects in the soil layer.

5. SUMMARY

The radiative transfer data sets were generated by using the ground based multi-frequency dual-polarization microwave radiometer, GBMR-6. The experiment results show that the volume scattering extinction effects of soil particles should be taken into account modeling the microwave radiative transfer process of dry soil media.

The numerical simulation results achieved using the dense media radiative transfer model demonstrate its reasonable applicability to the dry soil, while there are still several problems needed to be addressed.

Future studies will include series experiments using the absorber as background and uniform size particles as overlaying materials. The experiment results will be used to analyze the volume scattering effects and particle size parameter quantitatively.

ACKNOWLEDGMENT:

This study was carried out as part of the Coordinated Enhanced Observing Period (CEOP) and Verification Experiment for AMSR/AMSR-E

funded by the Japanese Science and Technology Corporation for Promoting Science and Technology Japan and the Japan Aerospace Exploration Agency. The authors express their great gratitude to them.

Furthermore we would like to thank the Field Production Science Center in Graduate School of Agricultural and Life Sciences in the University of Tokyo, for providing us the possibility to conduct the field experiments in the university farm, Mr. Kouji Kuboda for his helping in field management.

REFERENCES

- 1) Eni G. Njoku, Thomas J. Jackson, Venkataraman Lakshmi, Tsz K. Chan., and Son V. Nghiem: Soil Moisture Retrieval From AMSR-E, *IEEE Trans. Geosci. Remote Sensing*, vol 41, pp. 215-229, February, 2003.
- 2) Eni G Njoku: AMSR Land Surface Parameters Algorithm Theoretical Basis Document (version 3.0), Jet Propulsion Laboratory, California Institute of Technology, Pasadena, CA, 1999.
- 3) Hui Lu, Toshio Koike, Hideyuki Fujii, Nozomu Hirose, and Katsunori Tamagawa: A Radiative Transfer Model and an Algorithm for Soil Moisture Including Very Dry Conditions, in *Proc. IGARSS 2005 Symposium*, Seoul, Korea, July 2005
- 4) Technical documents of Radiometer Physics GmbH: description 6 channel radiometer, Meckenheim, Germany. May, 1996
- 5) Schmugge, T. J., Kustas, W. P., Ritchie, J. C., Jackson, T. J. and Rango, A.: Remote Sensing in Hydrology, *Advances in Water Resources*, Vol.25, pp. 1367-1385, 2002
- 6) Ulaby, F. T., Moore, K. T. and Fung, A. K.: *Microwave Remote Sensing: Active and Passive, Volume III: From Theory to Application*, Artech House Publishers, 1986
- 7) M. C. Dobson, F. T. Ulaby, M. T. Hallikainen, and M. A. El-Rayes: Microwave Dielectric Behavior of Wet Soil—Part II: Dielectric Mixing Models, *IEEE Trans. Geosci. Remote Sensing*, vol. GE-23, No. 1, pp. 35-46, January, 1985.
- 8) P. S. Ray: Broadband Complex Refractive Indices of Ice and Water, *Applied Optics*, vol. 11, No. 8, pp. 1836-1844, August, 1972
- 9) G. Liu: A fast and accurate model for microwave radiance calculations, *Journal of the Meteorological Society of Japan*, vol. 76, no. 2, pp. 335-343, 1998
- 10) L. C. Henyey and J. L. Greenstein: Diffuse radiation in the galaxy, *Astrophysical Journal*, vol. 93, pp. 70-83, 1941
- 11) C. F. Bohren, D. R. Huffman: *Absorption and scattering of light by small particles*, Wiley & Sons, 1983.
- 12) Boheng Wen, Leung Tsang, Dale P. Winebrenner, and Akria Ishimura: Dense medium radiative transfer theory: comparison with experiment and application to microwave remote sensing and polarimetry, *IEEE Transactions on Geoscience and Remote Sensing*, Vol.28, NO. 1, pp. 46-59, January, 1990
- 13) Leung Tsang, Jin Au Kong: *Scattering of Electromagnetic Waves: Advanced Topics*, New York: Wiley, 2001.

(Received September 30, 2005)